

Precise Determination of the Strong Coupling Constant from Dijet Cross Sections up to the Multi-TeV Range

Fazila Ahmadova^{1,2}, Daniel Britzger¹, Xuan Chen³, Johannes Gäbler⁴, Aude Gehrmann-De Ridder^{5,2}, Thomas Gehrmann², Nigel Glover⁶, Claire Gwenlan⁷, Gudrun Heinrich⁸, Alexander Huss⁹, Lucas Kunz⁸,

João Pires^{10,11}, Klaus Rabbertz⁴ and Mark Sutton¹²

¹*Max-Planck-Institut für Physik, Boltzmannstraße 8, 85748 Garching, Germany*

²*Department of Physics, Universität Zürich, Winterthurerstrasse 190, CH-8057 Zürich, Switzerland*

³*School of Physics, Shandong University, Jinan, Shandong 250100, China*

⁴*Karlsruhe Institute of Technology (KIT), Institute for Experimental Particle Physics, Wolfgang-Gaede-Straße 1, 76131 Karlsruhe, Germany*

⁵*Institute for Theoretical Physics, ETH, Wolfgang-Pauli-Strasse 27, CH-8093 Zürich, Switzerland*

⁶*Institute for Particle Physics Phenomenology, University of Durham, Durham DH1 3LE, United Kingdom*

⁷*Department of Physics, The University of Oxford, Oxford OX1 3RH, United Kingdom*


⁸*Karlsruhe Institute of Technology (KIT), Institute for Theoretical Physics, Wolfgang-Gaede-Straße 1, 76131 Karlsruhe, Germany*

⁹*Theoretical Physics Department, CERN, CH-1211 Geneva 23, Switzerland*

¹⁰*LIP, Avenida Professor Gama Pinto 2, P-1649-003 Lisboa, Portugal*

¹¹*Faculdade de Ciências, Universidade de Lisboa, 1749-016 Lisboa, Portugal*

¹²*Department of Physics and Astronomy, The University of Sussex, Brighton BN1 9RH, United Kingdom*

 (Received 5 January 2025; revised 7 May 2025; accepted 22 May 2025; published 17 July 2025)

We determine the value of the strong coupling α_s and study its running over a wide range of scales as probed by the dijet production process at hadron colliders, based on a next-to-next-to-leading-order QCD analysis of LHC dijet data. From a large subset of these data a value of $\alpha_s(m_Z) = 0.1178 \pm 0.0022$ is obtained for the strong coupling at the scale of the Z-boson mass m_Z , using the invariant mass of the dijet system to select the scale where α_s is probed. The combination of different datasets enhances the reach and precision of the analysis in the multi-TeV range and allows for the first determination of α_s up to scales of 7 TeV. Complementing the LHC data with dijet cross sections measured at the HERA electron–proton collider, the kinematic range is extended to test the running of the strong coupling toward smaller scales. Our results exhibit excellent agreement with predictions based on the renormalization group equation of QCD, and represent a comprehensive test of the asymptotic behavior of QCD, spanning more than three orders of magnitude in energy scale.

DOI: 10.1103/PhysRevLett.135.031903

Introduction—The theory of quantum chromodynamics (QCD) [1–5] so far successfully describes the dynamics and asymptotic behavior of the strong interaction. The renormalization group equation (RGE) of QCD predicts the scale evolution (“running”) of its coupling α_s . Consequently, the determination of the strong coupling at different energy scales probes the non-Abelian gauge structure of QCD. Despite its outstanding importance as the only free parameter of massless QCD, the value of the strong coupling constant at the reference scale of the Z-boson mass $\alpha_s(m_Z)$ is known with an uncertainty of approximately 1% [6] and hence is one of the least precisely determined fundamental constants in physics.

In this Letter, we make use of new precise predictions from perturbative QCD (pQCD) for dijet production at next-to-next-to-leading order (NNLO), including subleading color contributions [7–9] to determine the value of the strong coupling constant $\alpha_s(m_Z)$. We use precise dijet production data recorded by the ATLAS [10,11] and CMS [12–14] experiments in proton–proton collisions (pp) at the LHC at center-of-mass energies of 7, 8, and 13 TeV. The analysis is further extended to include dijet cross sections measured in electron–proton (ep) collisions at the HERA collider [15–19], which operated at considerably lower center-of-mass energies of $\sqrt{s} = 300$ and 320 GeV. This allows the investigation of the running of the strong coupling $\alpha_s(\mu_R)$ over energy scales ranging from a few GeV to the TeV regime. The first theoretical studies of dijet production were performed at next-to-leading order in pQCD in Refs. [20,21]. The first applications of NNLO predictions to determine α_s were carried out using e^+e^- event shape data in Ref. [22] and using deep-inelastic

Published by the American Physical Society under the terms of the Creative Commons Attribution 4.0 International license. Further distribution of this work must maintain attribution to the author(s) and the published article's title, journal citation, and DOI. Funded by SCOAP³.

TABLE I. Selected dijet datasets with center-of-mass energy \sqrt{s} , cross-section definition $d\sigma$, jet size parameter R , and integrated luminosity \mathcal{L} .

Data	\sqrt{s} [TeV]	$d\sigma$	R	\mathcal{L}
ATLAS [10]	7	$(d^2\sigma/dm_{jj}dy^*)$	0.6	$4.5 \text{ fb}^{-1} \pm 1.8\%$
CMS [12]	7	$(d^2\sigma/dm_{jj}dy_{\text{max}})$	0.7	$5.0 \text{ fb}^{-1} \pm 2.2\%$
CMS [13]	8	$(d^3\sigma/d\langle p_T \rangle_{1,2} dy^* dy_b)$	0.7	$19.7 \text{ fb}^{-1} \pm 2.6\%$
ATLAS [11]	13	$(d^2\sigma/dm_{jj}dy^*)$	0.4	$3.2 \text{ fb}^{-1} \pm 2.1\%$
CMS [14]	13	$(d^2\sigma/dm_{jj}dy_{\text{max}})$	0.8	$33.5 \text{ fb}^{-1} \pm 1.2\%$
CMS [14]	13	$(d^3\sigma/dm_{jj}dy^* dy_b)$	0.8	$29.6 \text{ fb}^{-1} \pm 1.2\%$

scattering (DIS) jet production in Ref. [23]. Recent determinations of α_s in pp collisions were performed at NNLO in a leading-color approximation with inclusive jet and dijet cross sections [14,24–26], in aN^3LO [27], and with multijet transverse energy correlations based on three-jet NNLO predictions [28–30]. Extending to 4.2 TeV, these predictions allow the measurement of α_s at the largest scales attained until now. By using multiple dijet datasets, our analysis achieves a considerably higher reach and resolution above scales of 1 TeV, allowing a measurement of α_s with unprecedented precision in the range beyond 1 TeV, extending as far as 7 TeV.

Methodology—The value of $\alpha_s(\mu_R)$ is determined by performing a least-squares minimization of the complete NNLO pQCD predictions for selected inclusive dijet cross-sections from the ATLAS and CMS experiments at pp center-of-mass energies \sqrt{s} of 7, 8, and 13 TeV, summarized in Table I. Two measurements from ATLAS at $\sqrt{s} = 7$ and 13 TeV are available as functions of the dijet mass $m_{jj} = \sqrt{(p_{j_1} + p_{j_2})^2}$, and half of the absolute rapidity separation $y^* = |y_1 - y_2|/2$, where p_{j_1}, p_{j_2} and y_1, y_2 denote the four-momenta and rapidities, respectively, of the two jets leading in p_T . Double-differential measurements have been performed by CMS at $\sqrt{s} = 7$ and 13 TeV, as functions of m_{jj} and the maximum absolute rapidity, y_{max} , of either of the two leading p_T jets. CMS has also published triple-differential cross sections at $\sqrt{s} = 8$ and 13 TeV as functions of either m_{jj} or the average transverse momentum of the two leading jets, $\langle p_T \rangle_{1,2}$, half of their rapidity separation y^* , and the longitudinal boost of the dijet system given by $y_b = |y_1 + y_2|/2$. These measurements employ the anti- k_t jet algorithm [31], but use different jet size parameters R . When cross sections are provided for more than one value of R , the larger jet size parameter is selected due to the expected improved perturbative convergence [32]. The CMS 13 TeV data are provided in both double- and triple-differential forms, but only one of the two datasets can be considered in the combined study because of their experimental correlations. We choose the double-differential variant in the following

due to its larger range in m_{jj} . In order to reduce the sensitivity to parton distribution functions (PDFs), the selected data are restricted to $y^* < 2.0$ (respectively $y_{\text{max}} < 2.0$) and $y_b < 1.0$, thereby excluding asymmetric parton configurations, where one parton carries a much smaller momentum fraction x than the other. As an example, in the 8 TeV data, this selection effectively restricts the PDFs to $x > 10^{-2}$ [34]. The selected data then have further experimental advantages since in the selected regions the tracking detectors of the experiments can be used. Finally, altogether 367 out of 493 cross-section measurements are considered in the α_s determination.

The dijet data are confronted with predictions in the framework of pQCD at NNLO [33–35] as implemented in the NNLOJET framework [36–38]. The α_s sensitivity in this calculation arises from two components: the hard matrix elements and the PDFs. The NNLO predictions include the full set of contributions, in particular all sub-leading-color parts [7–9], which are, for the first time, used in the determination of α_s with LHC jet data. Using the APPLfast library [24,39], the NNLO pQCD coefficients are stored independently of the $\alpha_s(m_Z)$ value and PDF. The statistical uncertainty, derived from the Monte Carlo integration in NNLOJET, is typically around a percent or below. The momentum distribution of partons inside the incoming proton is obtained from PDFs. The x dependence of the PDFs is defined at a starting scale μ_0 , and the PDFs are evolved to the factorization scale μ_F using Dokshitzer-Gribov-Lipatov-Altarelli-Parisi (DGLAP) evolution, with α_s as a free parameter, where they are convolved with the hard coefficients. We set the scale μ_0 to 90 GeV, a characteristic hard scale, and the x dependence is taken from the PDF4LHC21 PDF combination [40]. The predictions further include bin-wise correction factors for non-perturbative effects (NP) and higher-order electroweak (EW) contributions [41]. Both correction factors and their uncertainties are taken as published by the experimental collaborations [10–14]. Further details on the evaluation of the theory predictions are collected in Appendix A. A comprehensive study to assess the agreement between the NNLO pQCD predictions and the dijet data, as well as the consistency of individual datasets across different kinematic regions and between multiple datasets is provided in Ref. [42]. Overall, good agreement is observed between the predictions and the data in all kinematic regions and for all datasets, with a very good consistency between the datasets.

The value of $\alpha_s(m_Z)$ is then determined through a least-squares fit of the NNLO predictions to the dijet data, similar to the method used in Refs. [23,39]. The uncertainties considered in the fit include experimental, NP, NNLO statistical, and PDF uncertainties. Their covariance matrices also take correlations between data points and datasets into account. Henceforth, the linearly propagated uncertainty from that fit will be denoted as “(fit,PDF)”

uncertainty to emphasize that this uncertainty comprises experimental and PDF related uncertainties together. Details on the χ^2 minimization and considerations on the PDF uncertainties are discussed in Appendix B.

The predictions are associated with further uncertainties, related to the value of $\alpha_s(m_Z)$ as used in the PDF determination and to the starting scale of the PDF evolution μ_0 . Since a variation in the factorization scale and $\alpha_s(m_Z)$ are related in the DGLAP framework, we apply the following approach. The starting scale is chosen corresponding to the bulk of the collider data entering into the PDF determination. A variation of $\alpha_s(m_Z)$ in the original PDF determination is then expected to be mirrored by a μ_0 variation, and vice versa. To validate this, we study additional fits, where the choice of the starting scale μ_0 is varied by factors of 0.5 and 2, or where we select PDFs that were determined with values of $\alpha_s(m_Z)$ varied by ± 0.001 . We find that these variations yield very similar uncertainties. In order to represent these two theoretical uncertainty components, we report half of the difference between two fits with μ_0 varied by factors of 0.5 or 2 as an uncertainty (denoted as “ (μ_0) ”).

An additional scale uncertainty accounts for missing higher orders beyond NNLO and for the actual choice of the renormalization μ_R and factorization μ_F scales. Since the uncertainty associated with this choice is theoretical in nature and reflects the sensitivity of the prediction to unphysical scale choices, it cannot be constrained by data and is therefore not included in the χ^2 function of the fit. It is derived by varying μ_R and μ_F independently by factors of 0.5, 1, or 2 around the central value $\mu_R = \mu_F = m_{\text{ij}}$ in the complete NNLO pQCD predictions, omitting the two variations of (0.5,2) and (2,0.5), i.e., using the so-called seven-point scale variations. Half of the difference between the largest and smallest prediction is reported as *scale* uncertainty (denoted as “ (μ_R, μ_F) ”), since the asymmetry in these variations is typically small.

Results from LHC dijets—The value of the strong coupling at the scale m_Z [6] is determined from the five LHC dijet datasets using complete NNLO pQCD predictions. The fit exhibits an excellent consistency with $\chi^2/n_{\text{d.o.f.}} = 0.92$ and the value of $\alpha_s(m_Z)$ is determined to be

$$\alpha_s(m_Z) = 0.1178(14)_{(\text{fit,PDF})}(1)_{(\mu_0)}(17)_{(\mu_R, \mu_F)}.$$

Fits of $\alpha_s(m_Z)$ were also performed for individual datasets. The results are collected in Table II and displayed in Fig. 1, where they are compared to the combined fit from all five datasets and to the world average value [6].

The results from the individual datasets exhibit (fit,PDF) uncertainties in the range between ± 0.0020 and ± 0.0039 . Datasets with larger integrated luminosity or at higher center-of-mass energy yield smaller uncertainties. The $\alpha_s(m_Z)$ values are consistent with the world average value.

TABLE II. Results of $\alpha_s(m_Z)$ from fits of complete NNLO pQCD predictions to dijet cross-section data. Listed are the values of $\alpha_s(m_Z)$ with the (fit,PDF) uncertainty, the (μ_0) uncertainty, and the scale uncertainty (μ_R, μ_F) . The upper rows display results from fits to individual datasets. The middle rows show results from fits to all studied LHC dijet data using the double-differential (2D) or triple-differential (3D) CMS 13 TeV data. The bottom rows show results from fits to HERA dijet data and from fits to LHC and HERA dijet data taken together.

Dataset	$\chi^2/n_{\text{d.o.f.}}$	$\alpha_s(m_Z)$
ATLAS 7 TeV	74.7/77	0.1193(33)(4)(6)
ATLAS 13 TeV	87.7/106	0.1145(32)(4)(16)
CMS 7 TeV	50.7/45	0.1151(39)(1)(9)
CMS 8 TeV	37.0/56	0.1173(25)(1)(11)
CMS 13 TeV (2D)	71.6/78	0.1209(25)(2)(20)
CMS 13 TeV (3D)	137.7/112	0.1181(20)(1)(15)
LHC dijets (CMS13-2D)	335.3/366	0.1178(14)(1)(17)
LHC dijets (CMS13-3D)	397.9/400	0.1172(14)(1)(14)
HERA	92.8/118	0.1177(14)(1)(34)
LHC + HERA (CMS13-2D)	428.4/485	0.1180(10)(1)(22)
LHC + HERA (CMS13-3D)	491.0/519	0.1177(10)(1)(24)

It is observed that the determination of $\alpha_s(m_Z)$ using all five LHC dijet datasets benefits significantly from independent measurements, extended kinematic ranges, and multiple center-of-mass energies. Hence, the experimental uncertainties are found to be reduced in the combined determination in comparison to any individual dataset.

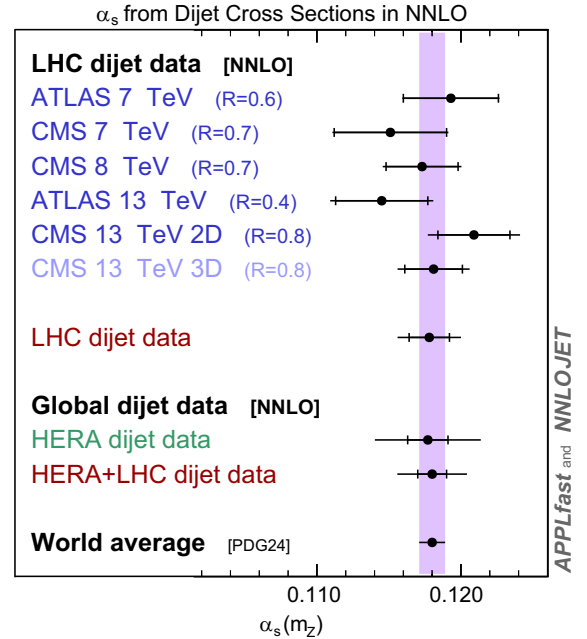


FIG. 1. Comparison of $\alpha_s(m_Z)$ determinations from dijet cross sections to the world average value. The inner error bars indicate the (fit,PDF) uncertainty, and the outer error bars further include the scale and μ_0 uncertainty.

An additional variant of the nominal fit using the CMS 3D data is presented in Appendix C.

Including HERA dijet data—The analysis is extended by further including data for dijet production in neutral-current DIS (NC DIS) taken at the HERA ep collider. These data, from the H1 [15,16,18,19] and ZEUS [17] collaborations, have previously been used for α_s determinations at NNLO accuracy [23,43,44] using the complete NNLO pQCD predictions [39,45,46]. Further details on the data are collected in Appendix D and the results of a fit to the HERA dijet measurements alone is presented in Table II. Using the HERA data provides competitive (fit,PDF) uncertainties in $\alpha_s(m_Z)$, but the fit exhibits a sizable scale dependence.

A combined fit to LHC and HERA dijet data is performed by considering all data and their uncertainties in the χ^2 function. Correlations between the dijet ep and pp processes arise from the PDF uncertainties. Since the scale dependence is specific to each process, the scale uncertainty is evaluated in separate fits by applying the seven-point scale variation procedure independently for either the pp or the ep calculation. The full scale uncertainty is then obtained by adding quadratically the scale uncertainties derived individually for each process.

In the combined fit, altogether 612 dijet cross-section data values are available. After applying the y^* , y_b , and y_{\max} data selection criteria, 486 data points remain for the combined fit, which yields

$$\alpha_s(m_Z) = 0.1180(10)_{(\text{fit,PDF})}(1)_{(\mu_0)}(22)_{(\mu_R, \mu_F)}$$

with $\chi^2/n_{\text{d.o.f.}} = 0.88$. The χ^2 value suggests an excellent consistency between the HERA and LHC data, as well as an outstanding agreement between data and the NNLO pQCD predictions. The α_s value is found to be in excellent agreement with the world average value of $\alpha_s(m_Z)$ of 0.1180 (9) [6]. As expected, the experimental uncertainties are reduced in the combined fit as compared to the fits to HERA or LHC data alone. The individual scale uncertainty from the pp NNLO calculations is found to be ± 0.0011 , and from ep it amounts to ± 0.0019 . While each of these scale uncertainties is smaller than what was obtained for the separate fits to the individual datasets (± 0.0017 for pp and ± 0.0034 for ep ; see Table II), the resulting total scale uncertainty is larger than in the fit to LHC data alone.

Running of the strong coupling—The asymptotic behavior of the strong coupling is one of the key properties of QCD [2–4]. Its prediction needs to be validated with experimental data, for example by probing the running of $\alpha_s(\mu_R)$ by determining α_s at different values of μ_R . For such a study, dijet cross sections represent a particularly powerful opportunity, since the dijet system provides a natural choice for the renormalization scale μ_R , which in principle could be chosen freely. As before, for dijet production in pp collisions μ_R is identified with m_{jj} , while

TABLE III. Results for the running of the strong coupling. The values are reported for different μ_R intervals. The columns show the central μ_R value, the resulting value of $\alpha_s(m_Z)$, and the corresponding value of $\alpha_s(\mu_R)$. The brackets denote the (fit,PDF), the (μ_0) and the (μ_R, μ_F) uncertainty.

μ_R^{avg} [GeV]	$\alpha_s(m_Z)$	$\alpha_s(\mu_R)$
7.4	0.1214(28)(1)(66)	0.2013(82)(4)(196)
10.1	0.1207(15)(1)(53)	0.1840(37)(2)(130)
13.3	0.1171(15)(0)(37)	0.1654(31)(0)(77)
17.2	0.1151(20)(0)(26)	0.1530(36)(1)(47)
20.1	0.1160(20)(1)(27)	0.1498(34)(1)(46)
24.5	0.1159(18)(0)(23)	0.1442(29)(1)(37)
29.3	0.1175(23)(0)(22)	0.1418(33)(0)(32)
36.0	0.1171(26)(0)(24)	0.1362(35)(1)(33)
49.0	0.1157(26)(1)(16)	0.1275(31)(1)(20)
77.5	0.1105(37)(3)(12)	0.1131(39)(3)(12)
250	0.1180(15)(1)(14)	0.1025(11)(1)(11)
370	0.1181(15)(1)(16)	0.0975(10)(1)(11)
550	0.1174(15)(1)(19)	0.0925(9)(1)(12)
810	0.1173(15)(2)(21)	0.0885(9)(1)(11)
1175	0.1171(16)(2)(23)	0.0848(8)(1)(12)
1760	0.1171(17)(2)(25)	0.0813(8)(1)(12)
2545	0.1171(18)(2)(27)	0.0783(8)(1)(12)
3490	0.1171(20)(2)(29)	0.0760(8)(1)(12)
4880	0.1185(31)(3)(34)	0.0742(12)(1)(13)
7040	0.1232(128)(12)(37)	0.0734(43)(4)(13)

for ep data $\mu_R^2 = Q^2 + \langle p_T \rangle_{1,2}^2$ [23] is used. The μ_R values of the HERA and LHC dijet cross sections span over three orders of magnitude from about 7 GeV up to 7 TeV.

Each cross-section measurement is then assigned a single representative value of μ_R . These values are used (only) to group the data into 20 distinct μ_R intervals. It is confirmed that in each μ_R interval, data from multiple datasets are considered.

We then perform a single fit to all dijet data, where, for each of the individual ranges of m_{jj} , a separate $\alpha_s(m_Z)$ value is used for the prediction. In this fit, the assumption of the QCD running enters in each interval only within a very limited range, and in the evolution of the PDFs from μ_0 to μ_F (using $\mu_0 = 90$ GeV and $\mu_F = \mu_R$). The technical fit parameter of $\alpha_s(m_Z)$ in each interval is evolved to the appropriate scale value $\alpha_s(\mu_R)$ as needed for the computation of the NNLO prediction. The advantage of a single fit to determine multiple $\alpha_s(m_Z)$ values at a time, in comparison to an alternative approach where each value is determined in a separate fit [23,28], is that the inference benefits from constraints on the correlated experimental uncertainties, as well as on the PDF uncertainties. In addition, the uncertainties in the resulting $\alpha_s(m_Z)$ values have known correlations and these values can therefore be used in further analyses. It has to be noted, that the lowest μ_R interval needs to be considered with some care, since these data are below the $2m_b$ threshold, and thus our computations in the five flavor number scheme are at the

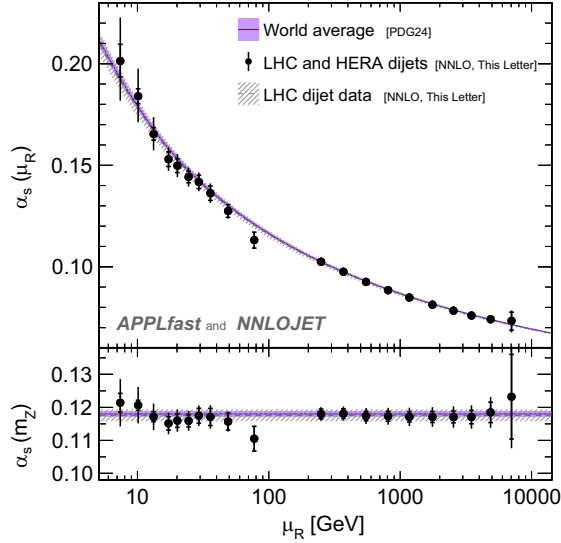


FIG. 2. Running of the strong coupling as a function of the chosen renormalization scale. The inner error bars indicate the (fit,PDF) uncertainty, and the outer error bars the total uncertainty. The upper panel displays the values $\alpha_s(\mu_R)$ and the lower panel displays the respective $\alpha_s(m_Z)$ value and the world average value [6]. The hatched area indicates the value of $\alpha_s(m_Z)$ from LHC dijet data and its running as a function of μ_R .

edge of their validity. However, it is found that these data do not impact other data in the fit, which is also seen from the resulting weak correlations, and thus this result can be neglected also at a later stage. The result at μ_R of 7.4 GeV is therefore reported here for completeness as in previous analyses [23,39].

The results from this single fit are presented in Table III and the related correlations of the (fit,PDF) uncertainty are listed in Appendix E. The results are compared to the expectation from the QCD RGE in Fig. 2, where in the lower panel the results of the 20 fit parameters for $\alpha_s(m_Z)$ are displayed, while the upper panel shows the respective values for $\alpha_s(\mu_R)$. The $\alpha_s(m_Z)$ values are evolved to the central value of each μ_R interval, illustrating the running of the strong coupling. Overall, excellent agreement with the expectation from the RGE running [when using the world average value for $\alpha_s(m_Z)$] is observed over the entire range from about 7 GeV up to 7 TeV. At scales of about a few hundred GeV, the size of the experimental and theoretical uncertainties are of similar size (about ± 0.0015), while in the TeV regime the experimental uncertainties dominate. In Fig. 3 our results are further compared to α_s extractions from inclusive jet and dijet data by the H1 and ZEUS collaborations at HERA [23,44], event shape observables at the PETRA or LEP e^+e^- colliders [47–50], a result from a global electroweak fit [6] and measurements of energy-energy correlations in pp collisions by ATLAS at the LHC [28]. Our results exhibit significantly smaller uncertainties and cover a significantly larger range in scale than any previous determination of $\alpha_s(\mu_R)$.

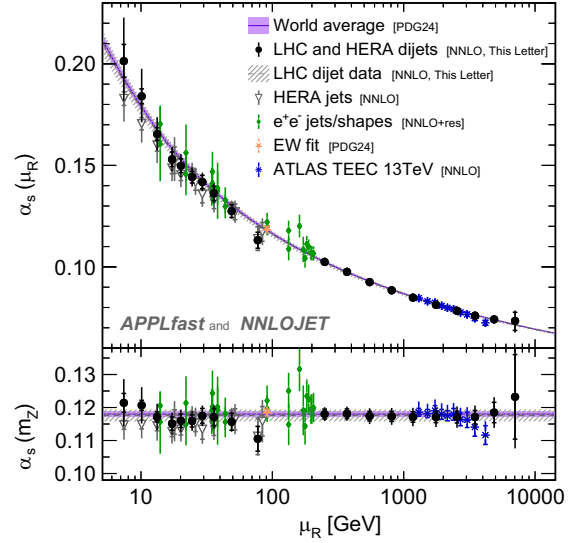


FIG. 3. Running of the strong coupling as a function of the chosen renormalization scale. The inner error bars indicate the (fit,PDF) uncertainty, and the outer error bars the total uncertainty. The upper panel displays the values $\alpha_s(\mu_R)$ and the lower panel displays the respective $\alpha_s(m_Z)$ value and the world average value [6]. The shaded area indicates the value of $\alpha_s(m_Z)$ from LHC dijet data and its running as a function of μ_R .

Summary—We have determined the strong coupling $\alpha_s(m_Z)$ from dijet data for the first time based on complete NNLO pQCD predictions. Using LHC data collected by the ATLAS and CMS collaborations at center-of-mass energies of 7, 8, and 13 TeV the strong coupling is determined to be

$$\alpha_s(m_Z) = 0.1178(22)_{(\text{tot})},$$

where experimental, PDF, and scale uncertainties are all of similar size. This value is consistent with the world average.

Including dijet cross sections measured in electron–proton collisions at the HERA collider makes this one of the most comprehensive and precise tests of the QCD renormalization group running of $\alpha_s(\mu)$ to date. The running is probed by a fit to individual m_{jj} ranges, and excellent agreement is found with the running predicted by QCD. Through the inclusion of both HERA and LHC data, the behavior of the strong coupling as a function of energy is tested over an unprecedented range, from about 7 GeV to 7 TeV. The presented results significantly improve our knowledge of the strong coupling in the TeV regime compared to previous determinations.

Note added—Recently, the CMS Collaboration released a determination of α_s and its running in the range $103 \text{ GeV} < \mu_R < 1600 \text{ GeV}$ using inclusive jet data at the LHC at various \sqrt{s} [51] in addition to HERA DIS data. Their determination make use of NNLO pQCD

predictions in the leading-color approximation. Their results are in agreement with ours.

Acknowledgments—This research was supported in part by the German Federal Ministry of Education and Research (BMBF) under Grant No. 05H21VKCCA, by the UK Science and Technology Facilities Council, by the Swiss National Science Foundation (SNF) under Contracts 200021-197130 and 200020-204200, by the National Science Foundation of China (Grants No. 12475085 and No. 12321005), by the Research Executive Agency (REA) of the European Union through the ERC Advanced Grant MC@NNLO (340983) and ERC Advanced Grant TOPUP (101019620) and by the Fundação para a Ciência e Tecnologia (FCT-Portugal), through the programmatic funding of R&D units reference UIDP/50007/2020 and under project CERN/FIS-PAR/0032/2021. C. G. and M. S. were supported by the IPPP Associateship program for this project. The authors acknowledge support by the state of Baden-Württemberg through bwHPC and the German Research Foundation (DFG) through Grant No. INST 39/963-1 FUGG (bwForCluster NEMO and bwUniCluster). The authors gratefully acknowledge the computing time provided on the high-performance computer HoreKa by the National High-Performance Computing Center at KIT (NHR@KIT). We also thank the CERN, DESY, and MPCDF computing facilities for providing computational resources.

Data availability—Some of the data that support the findings of this Letter are openly available. The value of the strong coupling for different values of the renormalization scale and their correlations are available within the Letter.

-
- [1] H. Fritzsch, M. Gell-Mann, and H. Leutwyler, *Phys. Lett.* **47B**, 365 (1973).
 - [2] D. J. Gross and F. Wilczek, *Phys. Rev. D* **8**, 3633 (1973).
 - [3] D. J. Gross and F. Wilczek, *Phys. Rev. Lett.* **30**, 1343 (1973).
 - [4] H. D. Politzer, *Phys. Rev. Lett.* **30**, 1346 (1973).
 - [5] F. Gross *et al.*, *Eur. Phys. J. C* **83**, 1125 (2023).
 - [6] S. Navas *et al.* (Particle Data Group), *Phys. Rev. D* **110**, 030001 (2024).
 - [7] M. Czakon, A. van Hameren, A. Mitov, and R. Poncelet, *J. High Energy Phys.* **10** (2019) 262.
 - [8] X. Chen, T. Gehrmann, E. W. N. Glover, A. Huss, and J. Mo, *J. High Energy Phys.* **09** (2022) 025.
 - [9] X. Chen, T. Gehrmann, E. W. N. Glover, and J. Mo, *J. High Energy Phys.* **10** (2022) 040.
 - [10] G. Aad *et al.* (ATLAS Collaboration), *J. High Energy Phys.* **05** (2014) 059.
 - [11] M. Aaboud *et al.* (ATLAS Collaboration), *J. High Energy Phys.* **05** (2018) 195.
 - [12] S. Chatrchyan *et al.* (CMS Collaboration), *Phys. Rev. D* **87**, 112002 (2013); **87**, 119902(E) (2013).
 - [13] A. M. Sirunyan *et al.* (CMS Collaboration), *Eur. Phys. J. C* **77**, 746 (2017).
 - [14] A. Hayrapetyan *et al.* (CMS Collaboration), *Eur. Phys. J. C* **85**, 72 (2025).
 - [15] C. Adloff *et al.* (H1 Collaboration), *Eur. Phys. J. C* **19**, 289 (2001).
 - [16] F. D. Aaron *et al.* (H1 Collaboration), *Eur. Phys. J. C* **67**, 1 (2010).
 - [17] H. Abramowicz *et al.* (ZEUS Collaboration), *Eur. Phys. J. C* **70**, 965 (2010).
 - [18] V. Andreev *et al.* (H1 Collaboration), *Eur. Phys. J. C* **75**, 65 (2015).
 - [19] V. Andreev *et al.* (H1 Collaboration), *Eur. Phys. J. C* **77**, 215 (2017); **81**, 739(E) (2021).
 - [20] Z. Kunszt and D. E. Soper, *Phys. Rev. D* **46**, 192 (1992).
 - [21] W. T. Giele, E. W. N. Glover, and J. Yu, *Phys. Rev. D* **53**, 120 (1996).
 - [22] G. Dissertori, A. Gehrmann-De Ridder, T. Gehrmann, E. W. N. Glover, G. Heinrich, and H. Stenzel, *J. High Energy Phys.* **02** (2008) 040.
 - [23] V. Andreev *et al.* (H1 Collaboration), *Eur. Phys. J. C* **77**, 791 (2017); **81**, 738(E) (2021).
 - [24] D. Britzger *et al.*, *Eur. Phys. J. C* **82**, 930 (2022).
 - [25] A. Tumasyan *et al.* (CMS Collaboration), *J. High Energy Phys.* **02** (2022) 142; **12** (2022) 035.
 - [26] CMS Collaboration, The strong coupling constant and its running from inclusive jet production at CMS, Report No. CMS-PAS-SMP-24-007, 2024, <http://cds.cern.ch/record/2912634>.
 - [27] T. Cridge, L. A. Harland-Lang, and R. S. Thorne, *Eur. Phys. J. C* **84**, 1009 (2024).
 - [28] G. Aad *et al.* (ATLAS Collaboration), *J. High Energy Phys.* **07** (2023) 085.
 - [29] M. Czakon, A. Mitov, and R. Poncelet, *Phys. Rev. Lett.* **127**, 152001 (2021); **129**, 119901(E) (2022).
 - [30] M. Alvarez, J. Cantero, M. Czakon, J. Llorente, A. Mitov, and R. Poncelet, *J. High Energy Phys.* **03** (2023) 129.
 - [31] M. Cacciari, G. P. Salam, and G. Soyez, *J. High Energy Phys.* **04** (2008) 063.
 - [32] J. Currie, A. Gehrmann-De Ridder, T. Gehrmann, N. Glover, A. Huss, and J. Pires, *J. High Energy Phys.* **10** (2018) 155.
 - [33] J. Currie, E. W. N. Glover, and J. Pires, *Phys. Rev. Lett.* **118**, 072002 (2017).
 - [34] A. Gehrmann-De Ridder, T. Gehrmann, E. W. N. Glover, A. Huss, and J. Pires, *Phys. Rev. Lett.* **123**, 102001 (2019).
 - [35] J. Currie, A. Gehrmann-De Ridder, T. Gehrmann, E. W. N. Glover, A. Huss, and J. Pires, *Phys. Rev. Lett.* **119**, 152001 (2017).
 - [36] A. Gehrmann-De Ridder, T. Gehrmann, N. Glover, A. Huss, and T. A. Morgan, *Proc. Sci. RADCOR2015* (2016) 075 [arXiv:1601.04569].
 - [37] T. Gehrmann *et al.*, *Proc. Sci. RADCOR2017* (2018) 074 [arXiv:1801.06415].
 - [38] A. Huss *et al.*, arXiv:2503.22804.
 - [39] D. Britzger *et al.*, *Eur. Phys. J. C* **79**, 845 (2019); **81**, 957(E) (2021).

- [40] R. D. Ball *et al.* (PDF4LHC Working Group), *J. Phys. G* **49**, 080501 (2022).
- [41] S. Dittmaier, A. Huss, and C. Speckner, *J. High Energy Phys.* **11** (2012) 095.
- [42] See Supplemental Material at <http://link.aps.org/supplemental/10.1103/knrv-2r3t> for the consistency study.
- [43] I. Abt *et al.* (H1 and ZEUS Collaborations), *Eur. Phys. J. C* **82**, 243 (2022).
- [44] I. Abt *et al.* (ZEUS Collaboration), *Eur. Phys. J. C* **83**, 1082 (2023).
- [45] J. Currie, T. Gehrmann, and J. Niehues, *Phys. Rev. Lett.* **117**, 042001 (2016).
- [46] J. Currie, T. Gehrmann, A. Huss, and J. Niehues, *J. High Energy Phys.* **07** (2017) 018; **12** (2020) 042.
- [47] G. Dissertori, A. Gehrmann-De Ridder, T. Gehrmann, E. W. N. Glover, G. Heinrich, G. Luisoni, and H. Stenzel, *J. High Energy Phys.* **08** (2009) 036.
- [48] S. Bethke, S. Kluth, C. Pahl, and J. Schieck (JADE Collaboration), *Eur. Phys. J. C* **64**, 351 (2009).
- [49] J. Schieck, S. Bethke, S. Kluth, C. Pahl, and Z. Trocsanyi (JADE Collaboration), *Eur. Phys. J. C* **73**, 2332 (2013).
- [50] G. Abbiendi *et al.* (OPAL Collaboration), *Eur. Phys. J. C* **71**, 1733 (2011).
- [51] V. Chekhovsky *et al.* (CMS Collaboration), *Phys. Lett. B* **868**, 139651 (2025).
- [52] O. V. Tarasov, A. A. Vladimirov, and A. Y. Zharkov, *Phys. Lett. B* **93**, 429 (1980).
- [53] S. A. Larin and J. A. M. Vermaseren, *Phys. Lett. B* **303**, 334 (1993).
- [54] B. Schmidt and M. Steinhauser, *Comput. Phys. Commun.* **183**, 1845 (2012).
- [55] A. Vogt, S. Moch, and J. A. M. Vermaseren, *Nucl. Phys. B* **691**, 129 (2004).
- [56] S. Moch, J. A. M. Vermaseren, and A. Vogt, *Nucl. Phys. B* **688**, 101 (2004).
- [57] V. Bertone, S. Carrazza, and J. Rojo, *Comput. Phys. Commun.* **185**, 1647 (2014).
- [58] V. Bertone, *Proc. Sci. DIS2017* (**2018**) 201 [arXiv:1708.00911].
- [59] T. Carli, G. P. Salam, and F. Siegert (Geneva, Switzerland, 2005), A posteriori inclusion of PDFs in NLO QCD final-state calculations, p. 110, arXiv:hep-ph/0510324.
- [60] T. Carli, D. Clements, A. Cooper-Sarkar, C. Gwenlan, G. P. Salam, F. Siegert, P. Starovoitov, and M. Sutton, *Eur. Phys. J. C* **66**, 503 (2010).
- [61] T. Kluge, K. Rabbertz, and M. Wobisch, *Conf. Proc. DIS2006*, 483 (2006).
- [62] D. Britzger, K. Rabbertz, F. Stober, and M. Wobisch, *DIS2012, Conf. Proc.* **217** (2012).
- [63] T. Sjöstrand, S. Mrenna, and P. Z. Skands, *J. High Energy Phys.* **05** (2006) 026.
- [64] T. Sjostrand, S. Mrenna, and P. Z. Skands, *Comput. Phys. Commun.* **178**, 852 (2008).
- [65] M. Bahr *et al.*, *Eur. Phys. J. C* **58**, 639 (2008).
- [66] J. Bellm *et al.*, *Eur. Phys. J. C* **76**, 196 (2016).
- [67] F. James and M. Roos, *Comput. Phys. Commun.* **10**, 343 (1975).
- [68] R. Brun and F. Rademakers, *Nucl. Instrum. Methods Phys. Res., Sect. A* **389**, 81 (1997).
- [69] A. Buckley, J. Ferrando, S. Lloyd, K. Nordström, B. Page, M. Rüfenacht, M. Schönherr, and G. Watt, *Eur. Phys. J. C* **75**, 132 (2015).
- [70] S. Bailey, T. Cridge, L. A. Harland-Lang, A. D. Martin, and R. S. Thorne, *Eur. Phys. J. C* **81**, 341 (2021).
- [71] R. D. Ball *et al.* (NNPDF Collaboration), *Eur. Phys. J. C* **77**, 663 (2017).
- [72] T.-J. Hou *et al.*, *Phys. Rev. D* **103**, 014013 (2021).
- [73] S. Alekhin, J. Blümlein, S. Moch, and R. Placakyte, *Phys. Rev. D* **96**, 014011 (2017).
- [74] R. D. Ball *et al.* (NNPDF Collaboration), *Eur. Phys. J. C* **82**, 428 (2022).
- [75] H. Abramowicz *et al.* (H1 and ZEUS Collaborations), *Eur. Phys. J. C* **75**, 580 (2015).

End Matter

Appendix A: Theory predictions—The pQCD cross section for the process with two initial-state hadrons is obtained from the factorization formula as the convolution of the PDFs of the incoming protons and the hard scattering cross section,

$$d\sigma = \sum_{a,b} \int \frac{dx_1}{x_1} \frac{dx_2}{x_2} f_a(x_1, \mu_F) f_b(x_2, \mu_F) d\hat{\sigma}_{ab}(\mu_R, \mu_F),$$

where $f_a(x, \mu_F)$ denotes the density of the partons of type a in the incoming proton at the factorization scale μ_F carrying the longitudinal momentum fraction x . Both contributions are sensitive to the value of α_s , as

$$d\hat{\sigma}_{ab}(\mu) \equiv d\hat{\sigma}_{ab}(\mu, \alpha_s(\mu)) \quad \text{and} \quad (\text{A1})$$

$$f_a(x, \mu) \equiv f_a(x, \mu, \alpha_s(\mu)). \quad (\text{A2})$$

The α_s dependence in the partonic cross section is explicit through the perturbative expansion, which for dijet production up to NNLO reads

$$\begin{aligned} d\hat{\sigma}_{ab}(\alpha_s) &= \left(\frac{\alpha_s(\mu)}{2\pi}\right)^2 d\hat{\sigma}_{ab,\text{LO}} + \left(\frac{\alpha_s(\mu)}{2\pi}\right)^3 d\hat{\sigma}_{ab,\text{NLO}} \\ &+ \left(\frac{\alpha_s(\mu)}{2\pi}\right)^4 d\hat{\sigma}_{ab,\text{NNLO}} + \mathcal{O}(\alpha_s^5(\mu)). \end{aligned} \quad (\text{A3})$$

The value of $\alpha_s(\mu)$ is obtained from $\alpha_s(m_Z)$ from the renormalization group running in the modified minimal subtraction ($\overline{\text{MS}}$) scheme, i.e., $\alpha_s(\mu) = \alpha_{s,\overline{\text{MS}}}^{(5)}(\mu, \alpha_s(m_Z))$, in three-loop order [52,53] as implemented in CRunDec [54]. The evolution is performed with $n_f = 5$ active flavors throughout, in particular also beyond the top-quark mass threshold. This is consistent with the perturbative calculation that does not include top-quark effects and thus effectively treats the top quark in the decoupling limit. The evolution of the PDFs with respect to a scale μ is governed by the DGLAP equations, whose splitting kernels \mathcal{P} depend on $\alpha_s(\mu)$,

$$\mu^2 \frac{df}{d\mu^2} = \mathcal{P}(\alpha_s) \otimes f. \quad (\text{A4})$$

The x dependence of the PDFs can be fixed at a starting scale μ_0 with value f_{μ_0} , and subsequently evolved to a scale μ using the DGLAP evolution,

$$f_a(x, \mu, \alpha_s) = [\Gamma(\mathcal{P}, \mu, \mu_0, \alpha_s) \otimes f_{\mu_0}]_a, \quad (\text{A5})$$

where Γ denotes the DGLAP kernels that are evaluated at three-loop order [55,56] using the program Apfel++ [57,58]. We set the scale μ_0 of the evolution to 90 GeV and the x dependence of $f_{\mu_0,x}$ is taken from PDF4LHC21 [40]. The NNLO cross section is obtained by integrating the dijet parton level predictions [Eq. (A3)] over the bin-dependent kinematic region Ω_i , $\sigma_{\text{NNLO},i} = \int_{\Omega_i} d\sigma$, using the dijet parton level matrix elements and phase-space integration routines implemented in NNLOJET. Our fit algorithm requires recalculating the predictions for different values of $\alpha_s(m_Z)$ and corresponding PDFs. To streamline this, NNLOJET is interfaced with the APPLfast library [24,39], which integrates the grid tools APPLgrid [59,60] and fastNLO [61,62]. The resulting interpolation grids for the dijet datasets typically have subpermille accuracy. The NNLO prediction is supplemented with additional correction factors to account for NP and higher-order EW contributions [41], c_{NP} and c_{EW} ,

$$\sigma_i = c_{\text{NP},i} \cdot c_{\text{EW},i} \cdot \sigma_{\text{NNLO},i}. \quad (\text{A6})$$

Both correction factors are taken as published by the experimental collaborations [10–14]. A consistent treatment of NP effects across all datasets is desirable but beyond the scope of this Letter. Hence, different hadronization and parton-shower models are applied, reflecting variations in the Monte Carlo event generators [63–66] used to derive $c_{\text{NP},i}$. Such variations are

considered by the collaborations in the assignment of uncertainties.

Appendix B: Fit algorithm and uncertainties—The objective function used in the fitting algorithm to determine the value of $\alpha_s(m_Z)$ is derived from normally distributed relative uncertainties and defined as [18]

$$\chi^2 = \sum_{i,j} \log \frac{\varsigma_i}{\sigma_i} (V_{\text{exp}} + V_{\text{NP}} + V_{\text{NNLOstat}} + V_{\text{PDF}})^{-1}_{ij} \log \frac{\varsigma_j}{\sigma_j},$$

where the double sum runs over all data points, ς_i denotes the measured cross section, σ_i denotes the theory prediction. The χ^2 is minimized using TMinuit's Migrad algorithm [67,68]. The covariance matrices V_{exp} , V_{NP} , V_{NNLOstat} , and V_{PDF} represent the relative experimental, NP, NNLO statistical, and PDF uncertainties, respectively. The experimental uncertainties are reported by the experimental collaborations and account for many systematic sources as well as statistical components including correlations from unfolding. Correlations between the experimental uncertainties of individual datasets are not provided and hence are assumed to be uncorrelated, which is certainly correct for the statistical components. A recent report from CMS [51] using inclusive jet data at different \sqrt{s} indicates that the dominating uncertainty from jet energy calibration and resolution may be considered as uncorrelated between such datasets, supporting that the omission of correlations is justified. The non-perturbative correction uncertainties are provided by the experimental collaborations and are derived using different Monte Carlo event generators and hadronization models, and from variations of their different respective model parameters. To represent both correlated and uncorrelated effects due to these various components, we follow the approach of Ref. [43], and assume a bin-to-bin correlation of 0.5. The NNLO statistical uncertainties originate from the Monte Carlo integration in NNLOJET and are typically at the percent level or below. The PDF uncertainties are obtained from the respective PDF set in the LHAPDF format [69], and evaluated at μ_0 . By considering them as a covariance matrix in χ^2 , the PDF uncertainties are further constrained by the jet data. The PDFs carry further uncertainties due to differing theoretical assumptions, data selections, and inference methods imposed by the PDF fitting groups. In the PDF4LHC21 PDF set, however, such differences are already included in the uncertainty representation [40] and represent differences between the MSHT [70], NNPDF3.1 [71], and CT18 [72] PDFs. Dedicated fits using these different PDF sets confirm that the PDF uncertainty indeed covers such differences. Results when using yet different PDFs, such

as ABMP [73], NNPDF4.0 [74], or HERAPDF2.0 [75], are typically found to be well within 2σ of the PDF uncertainty.

Appendix C: Fits using CMS 13 TeV triple-differential data—The CMS Collaboration reported dijet cross sections at $\sqrt{s} = 13$ TeV also in triple-differential variants as a function of y^* , y_b , and m_{jj} or $\langle p_T \rangle_{1,2}$ [14]. Besides observables and different binnings, the analyzed data and experimental methods are equivalent in these three variants, and therefore these datasets cannot be used in a fit together because of their experimental correlations. This section discusses the triple-differential measurement ($d^3\sigma/dm_{jj}dy^*dy_b$) for a determination of $\alpha_s(m_Z)$ instead of their double-differential variant (cf. Table I) When restricting the data to $y^* < 2.0$ and $y_b < 1.0$, similar to the fits in the “Methodology” section, the fit to these data results in a value of $\chi^2/n_{\text{d.o.f.}}$ of 1.23 for 113 data points and provides $\alpha_s(m_Z) = 0.1181(20)_{(\text{fit,PDF})}(1)_{(\mu_0)}(15)_{(\mu_R, \mu_F)}$. Using the triple-differential data as an alternative to the double-differential variant in the combined fit, the value

$$\alpha_s(m_Z) = 0.1172(14)_{(\text{fit,PDF})}(1)_{(\mu_0)}(14)_{(\mu_R, \mu_F)}$$

is derived with $\chi^2/n_{\text{d.o.f.}}$ of 0.99. The result is in good agreement with that obtained when using the double-differential data. For the main analysis presented in this Letter, the double-differential CMS data are chosen rather than the triple-differential cross sections, as the sensitivity to the PDF parameters is lower, and the double-differential data reaches higher values of m_{jj} , while the sensitivity of the data to $\alpha_s(m_Z)$ is similar.

Appendix D: Including HERA dijet data—We extend our analysis by further including data for inclusive dijet production in NC DIS reported by the H1 [15,16,18,19] and ZEUS [17] collaborations, together with complete NNLO pQCD predictions [39,45,46]. These data have already been used for α_s determinations at NNLO accuracy [23,43,44], and thus, the method and data selection from H1 [23] is closely followed: four datasets at $\sqrt{s} = 300$ and 320 GeV at lower or higher photon virtualities Q^2 being considered, and the fit methodology differing only in the choices for the PDF and μ_0 . In addition, data from the ZEUS collaboration recorded at $\sqrt{s} = 320$ GeV and for $Q^2 > 125$ GeV² are also included, similar to Refs. [43,44]. All five datasets, summarized in Table IV, employ the k_t jet algorithm with $R = 1.0$ and represent double-differential cross sections as a function of Q^2 and $\langle p_T \rangle_{1,2}$. The ZEUS data are restricted

TABLE IV. Summary of the HERA datasets for dijet production with the k_t jet algorithm with jet size parameter $R = 1.0$.

Dataset	\sqrt{s} [GeV]	Cuts
H1 300 GeV high- Q^2 [15]	300	
H1 HERA-I low- Q^2 [16]	320	$\mu > 2m_b$
H1 HERA-II low- Q^2 [19]	320	$\mu > 2m_b$
H1 HERA-II high- Q^2 [18]	320	
ZEUS HERA-I+II high- Q^2 [17]	320	$\langle p_T \rangle_{1,2} > 15$ GeV

to $\langle p_T \rangle_{1,2} > 15$ GeV to exclude infrared sensitive data points [46]. At lower Q^2 , data points with a typical scale smaller than twice the bottom quark mass ($\mu < 2m_b$) are excluded in the nominal fit, since the predictions are performed with $n_f = 5$ [23]. The correlations between datasets are described in Refs. [23,43]. The scales are identified with $\mu_R^2 = \mu_F^2 = Q^2 + \langle p_T \rangle_{1,2}^2$. From fits to individual datasets, consistent results are obtained for $\chi^2/n_{\text{d.o.f.}}$ and $\alpha_s(m_Z)$ for the H1 data as in Ref. [23]. For the ZEUS data a value of $\chi^2/n_{\text{d.o.f.}} = 11.8/15$ is obtained with $\alpha_s(m_Z) = 0.1164(33)_{(\text{fit,PDF})}(20)_{(\mu_R, \mu_F)}$. A fit to all HERA dijet data results in a value $\alpha_s(m_Z) = 0.1177(14)_{(\text{fit,PDF})}(1)_{(\mu_0)}(34)_{(\mu_R, \mu_F)}$ with $\chi^2/n_{\text{d.o.f.}} = 92.8/118$. As expected, these results are very similar to those reported from H1 data alone [23], as the ZEUS dijet data add only modestly to the sensitivity. These results represent the first determination of $\alpha_s(m_Z)$ at NNLO using only DIS dijet production, including data from H1 and ZEUS. The value of $\alpha_s(m_Z)$ as determined in a single fit to HERA and LHC dijet data taken together was reported in Table II. This analysis benefits from theory predictions for dijet production at NNLO and from independent, and thus fully uncorrelated, experimental setups. When the triple-differential data from CMS at 13 TeV are used instead of the double-differential variants in that fit, a value of $\alpha_s(m_Z)$ of

$$0.1177(10)_{(\text{fit,PDF})}(1)_{(\mu_0)}(27)_{(\mu_R, \mu_F)}$$

is obtained with $\chi^2/n_{\text{d.o.f.}}$ of 0.95 for 520 individual data points. This result is in good agreement with that obtained using the double-differential data instead.

Appendix E: Resulting correlations—The resulting correlations of the (fit,PDF) uncertainty in the combined fit of 20 parameters to the HERA and LHC dijet data are listed in Table V. These correlations originate from the combined determination of 20 fit parameters and from correlated uncertainties between individual cross-section values. In the region where HERA or LHC data

TABLE V. Correlations of the (fit,PDF) uncertainty from the fit of 20 $\alpha_s(m_Z)$ parameters to HERA and LHC dijet data.

μ_R [GeV]	Correlations																			
7.4		56	29	21	19	22	15	17	16	12	2	1	-1	-2	-3	-3	-3	-3	-1	0
10.1	56			65	50	49	50	37	38	36	23	9	8	5	2	0	-2	-3	-3	-2
13.3	29	65			58	52	54	40	45	39	23	11	11	9	7	5	2	1	0	1
17.2	21	50	58			48	52	39	44	41	24	9	9	8	7	5	3	2	1	1
20.1	19	49	52	48			52	39	38	41	24	9	9	9	8	7	5	4	2	1
24.5	22	50	54	52	52			55	49	53	36	10	11	11	10	9	7	5	3	2
29.3	15	37	40	39	39	55			41	44	33	6	8	9	10	9	8	7	5	3
36.0	17	38	45	44	38	49	41			39	28	5	6	8	8	8	8	7	5	3
49.0	16	36	39	41	41	53	44	39			31	4	5	6	7	8	7	6	5	3
77.5	12	23	23	24	24	36	33	28	31				1	2	2	3	4	4	3	2
250	2	9	11	9	9	10	6	5	4	0			90	87	83	78	71	64	54	36
370	1	8	11	9	9	11	8	6	5	1	90			95	91	87	80	72	61	40
550	-1	5	9	8	9	11	9	8	6	2	87	95			97	93	88	80	67	45
810	-2	2	7	7	8	10	10	8	7	2	83	91	97			97	93	86	74	49
1175	-3	0	5	5	7	9	9	8	8	3	78	87	93	97			97	92	80	55
1760	-3	-2	2	3	5	7	8	8	7	4	71	80	88	93	97			96	87	62
2545	-3	-3	1	2	4	5	7	7	6	4	64	72	80	86	92	96			92	70
3490	-3	-3	0	1	2	3	5	5	5	3	54	61	67	74	80	87	92			78
4880	-1	-2	0	1	1	2	3	3	3	2	36	40	45	49	55	62	70	78	...	30
7040	0	0	1	1	1	1	1	1	1	1	9	10	11	12	14	17	21	27	30	...

are important, μ_R smaller or larger 100 GeV, respectively, the correlations originate predominantly from correlated experimental systematic uncertainties. Hence, correlations are found to be positive. Correlations

between low and high scales, respectively between HERA and LHC data, originate from PDF uncertainties.

The additional (μ_0) and (μ_R, μ_F) uncertainties are fully correlated.